

Interlayer-glide-driven isosymmetric phase transition in compressed In_2Se_3

Feng Ke,^{1,2} Cailong Liu,¹ Yang Gao,³ Junkai Zhang,¹ Dayong Tan,^{2,4} Yonghao Han,¹ Yanzhang Ma,³ Jinfu Shu,⁵ Wenge Yang,^{2,5} Bin Chen,² Ho-Kwang Mao,^{2,5} Xiao-Jia Chen,² and Chunxiao Gao^{1,a)}

¹State Key Laboratory for Superhard Materials, Institute of Atomic and Molecular Physics, Jilin University, Changchun 130012, China

²Center for High Pressure Science and Technology Advanced Research, Shanghai 201203, China

³Department of Mechanical Engineering, Texas Tech University, Lubbock, Texas 79409, USA

⁴Guangzhou Institute of Geochemistry, Chinese Academy of Sciences, Guangzhou 510640, China

⁵Geophysical Laboratory, Carnegie Institution of Washington, Washington, DC 20015, USA

(Received 30 March 2014; accepted 14 May 2014; published online 28 May 2014)

We report an anomalous phase transition in compressed In_2Se_3 . The high-pressure studies indicate that In_2Se_3 transforms to a new isosymmetric $R\bar{3}m$ structure at 0.8 GPa whilst the volume collapses by $\sim 7\%$. This phase transition involves a pressure-induced interlayer shear glide with respect to one another. Consequently, the outer Se atoms of one sheet locate into the interstitial sites of three Se atoms in the neighboring sheets that are weakly connected by van der Waals interaction. Interestingly, this interlayer shear glide changes the stacking sequence significantly but leaves crystal symmetry unaffected. This study provides an insight to the mechanisms of the intriguing isosymmetric phase transition. © 2014 AIP Publishing LLC. [<http://dx.doi.org/10.1063/1.4879832>]

Phase transitions are ubiquitous in nature. Christy has classified the phase transitions rigorously into three types by symmetry criteria.¹ An additional type extension (type “0”) in which there is no change of space group or the occupied Wyckoff sites,¹ i.e., isosymmetric transition was proposed to incorporate into this scheme. The mechanism of the isosymmetric phase transition has been attracted considerable attention to both crystallographic scientists and physicists. Previous works suggest that this transition can arise from various kinds of changes in electronic structure of materials, for instance the charge transfer,² the high-spin to low-spin crossover,³ and so on. Besides, the change of coordination number can cause an isosymmetric transition as well.⁴ For organic materials, rearrangement of hydrogen bonds can also result in this type of transition.⁵ Recently, isosymmetric transitions induced by the distortion or rotation of octahedral sublattice have also been observed.^{6,7} Herein, we report an interesting finding: the interlayer shear glide-driven isosymmetric phase transition occurred with $\sim 7\%$ volume collapse in layered Indium selenide (In_2Se_3).

At ambient conditions, In_2Se_3 crystallizes into a rhombohedral (hexagonal setting) layered structure with covalent bonding between In and Se atoms within a layer. Neighboring layers are held together by van der Waals forces. One third of the possible In sites are vacant. Resulting from the large amount of intrinsic vacancy defects and much weaker van der Waals interaction than the in-plane covalent bonds, In_2Se_3 shows high anisotropy and is sensitive to surrounding environments.^{8,9} Several different polytypic structures have been observed in In_2Se_3 at room or high-temperature conditions.^{10–13} These phases show much different structural and electrical properties that are attractive for various applications including phase-change random access memory devices,¹⁴ photon detector.^{15,16} Despite great

efforts on structural and electrical properties of In_2Se_3 for decades, its ambient-condition structure remains confusing and contradictory.^{10,17–20} One possible reason is that X-ray diffraction (XRD) measurements in powders seem to be insensitive to closed symmetries, such as the centrosymmetric $R\bar{3}m$ and noncentrosymmetric $R3m$ symmetries. Furthermore, pressure or strain is a much more powerful controlling factor than temperature for driving transformations toward structures with higher density and smaller volume, and hence tuning properties of materials. So far, little is known about how compression affects the structural properties of In_2Se_3 . Previous study assigned the ambient- and high-pressure In_2Se_3 structures to $R\bar{3}m$ symmetry for consistency.²⁰ More information about In_2Se_3 , specially the transition mechanism is still unclear and needs further exploration.

In order to clarify the above mentioned issues, we conducted high-pressure studies of In_2Se_3 with combined experimental and theoretical methods. The experimental results show that confocal Raman spectra measurements can perfectly complement the insensibility of XRD in identifying the $R\bar{3}m$ and $R3m$ symmetries. To avoid uncertain experimental and Rietveld refinements error, first-principle geometry optimization calculations are employed to further justify the experimental results.

High-pressure angle-dispersive XRD spectra ($\lambda = 0.6199 \text{ \AA}$) were collected at beamline 15U1 of Shanghai Synchrotron Radiation Facility (SSRF) and beamline 4W2 of Beijing Synchrotron Radiation Facility (BSRF). For the experiments, In_2Se_3 powders (Alfa Aesar, purity 99.99%) and small piece of ruby, the pressure calibrant,²¹ were loaded into a diamond-anvil cell. Silicone oil was used as pressure transmitting medium. Distance between sample and detector, and parameters of detector were calibrated using a CeO_2 standard. Bragg diffraction images were integrated using FIT2D software, yielding one-dimensional intensity versus diffraction angle 2θ patterns. XRD patterns were fitted with Rietveld refinement through GSAS program package. High-pressure

^{a)}Author to whom correspondence should be addressed. Electronic mail: gaocx@jlu.edu.cn.

Raman spectra were collected with Renishaw InVia spectrometer using a 633 nm He-Ne laser and a 50 times Leica optical microscope.

First-principle calculations were performed on basis of the density functional theory, plane-wave, pseudopotential method on standard CASTEP program in Material Studio package.²² The electron exchange-correction energy was treated within the generalized gradient approximation (GGA), using the functional of Perdew, Burke, Ernzerhof.²³ A plane-wave cutoff energy of 500 eV, and appropriate Monkhorst-Pack k -point meshes ($5 \times 5 \times 5$ meshes) were set up for all structures to ensure the enthalpy calculations being well converged.

Figure 1(a) shows the selected XRD patterns of In_2Se_3 up to 12 GPa measured at room temperature. With gradually increasing pressure up to 0.8 GPa, some diffraction peaks such as (006), (1010), and (116) start to split up. Peak of (10-5) picks up its intensity rapidly, while the strongest (104) peak at ambient pressure loses its intensity dramatically in compression, which signals the I-II phase transition. Phase II remains stable up to 12.0 GPa, the highest pressure of this study. Upon quenching to ambient pressure, the diffraction pattern of phase II remains unchanged, indicating that the phase transition is irreversible. Recently reported work partially agrees with our results.²⁰

With the Rietveld refinement analysis through the GSAS program package (Fig. 1(b)), all the reflections of phase I can be indexed into a rhombohedral structure. It is found that the fitting with $R\bar{3}m$ symmetry (No. 166) is better than with other symmetries, matching well with the results

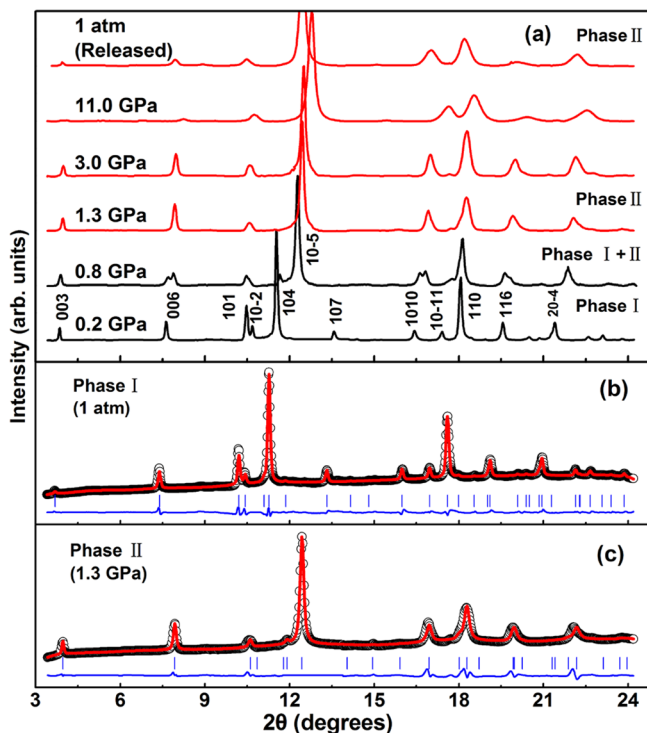


FIG. 1. (a) Representative XRD patterns (background subtracted) of In_2Se_3 at various pressures. (b) and (c) show the Rietveld refinement results through the GSAS program package for phase I at ambient pressure and phase II at 1.3 GPa, respectively. The solid lines and open circles represent the fitted and experimental data, respectively. The solid lines at the bottom are the residual intensities. The vertical bars indicate the peak positions.

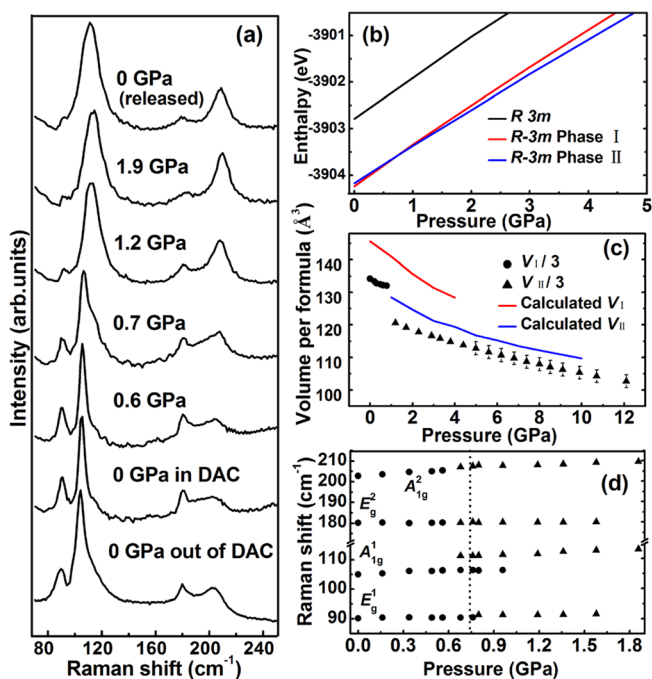


FIG. 2. (a) High-pressure Raman spectra of In_2Se_3 . (b) Pressure dependent enthalpies of phases I and II computed by first-principle calculation on standard CASTEP program in Material Studio package. (c) Volume versus pressure data for phases I and II obtained with XRD and geometry optimization. (d) Pressure dependent Raman-mode frequencies shift in In_2Se_3 .

of Popovic *et al.*¹⁰ We notice that others assigned $R3m$ symmetry to phase I.¹⁷⁻¹⁹ To clarify this, we carried out Raman spectra measurements (Fig. 2(a)), which may help to discover the subtle difference between them. The irreducible representations for $R\bar{3}m$ and $R3m$ symmetries are $\Gamma = 2A_{1g}(R) + 3A_{2u}(IR) + 2E_g(R) + 3E_u(IR)$ and $\Gamma = 5A_1(R, IR) + 5E(R, IR)$, respectively. Due to the loss of centrosymmetry in $R3m$ symmetry, the A_1 modes related to the intra-layer vibrations significantly split up,¹⁹ and one of them should be seen at $\sim 237 \text{ cm}^{-1}$ for In_2Se_3 with $R3m$ symmetry but not for that with $R\bar{3}m$ symmetry. As no obvious Raman peak is observed at $\sim 237 \text{ cm}^{-1}$ in our Raman results (Fig. 2(a)), we infer that the $R\bar{3}m$ structure is more suitable for phase I. The computed enthalpies curves based on first-principle calculation (Fig. 2(b)) confirm that the $R\bar{3}m$ structure is lower enthalpy and more stable than the $R3m$ structure.

The Rietveld refinement analysis reveals that the phase II still has $R\bar{3}m$ symmetry (Fig. 1(c)). The Raman spectra confirm this result as well. As shown in Fig. 2(a), the Raman modes of phase II are similar with those of phase I except for the difference in relative intensity and peak broadening, resembling the results in Ref. 20. The Raman results suggest that the symmetries of phases I and II are the same. In addition, the Raman spectra of phase II are also similar to that of the high-temperature phase, $\beta\text{-In}_2\text{Se}_3$, a rhombohedral structure with $R\bar{3}m$ symmetry.¹³ The calculated enthalpies curves for phases I and II cross over around 1 GPa (Fig. 2(b)), and the $R\bar{3}m$ structure of phase II becomes more stable than that of phase I. More detailed information is shown in supplementary material.²⁴ Hence, we consider that phase II is also a rhombohedral structure with the same $R\bar{3}m$ symmetry as

phase I. However, the volume of In_2Se_3 drops unexpectedly by $\sim 7\%$ after the phase transition (Fig. 2(c)), which is interesting. Pioneering work on chalcogenide inspires our understanding for the mechanism behind. Chalcogenide laminar materials with $R\bar{3}m$ symmetry have four Raman-active modes:²⁵ the lower frequency E_g mode is related to the shear vibrations between adjacent layers on a-b plane, the lower frequency A_{1g} mode arises from the vibrations of one layer against the others along c -axis, and the higher frequency E_g and A_{1g} modes result from the intralayer vibrations. An obvious blue shift in the A_{1g} mode at 104 cm^{-1} is observed along with the phase transition (Fig. 2(d)), which indicates that the interlayer interaction is significantly enhanced in phase II.

The fact that the space group of high-pressure In_2Se_3 (above 0.8 GPa) is the same as that of the low-pressure form, easily reminds one of an isosymmetric phase transition. Previous studies suggest that various kinds of electronic changes in materials can result in this type of phase transition. For instances, the localized-delocalized charge transfer,² the high-to-low-spin crossover.³ In case of In_2Se_3 , the $4d^{10}$ valance electrons of In are bounded in localized states, and the $4s^2$ electrons of Se show the strong characteristics of lone-pair electrons. The $5s^2$ electrons of In are located at the lower valance bands (Fig. 3(a)). With such an electronic configuration, it seems impossible to perform a charge transfer or a spin crossover at low pressures. Additionally, the charge transfer seems to occur continuously rather than abruptly,² which is not consistent with the rapid phase transition and volume reduction in In_2Se_3 . Therefore, we infer that the charge transfer or spin crossover in In_2Se_3 , if occurred, should not accounts for the I-II isosymmetric transition with such a sudden volume collapse.

According to Refs. 6 and 7, the isosymmetric transition may also relate to the rotation or distortions of octahedral sublattice. For In_2Se_3 , the in-plane In and Se atoms are connected with octahedral sublattice structure. We analyzed the structures of In_2Se_3 before and after the isosymmetric transition. In_2Se_3 has three types of chemical bonds. Two of them are covalent bonds (In-Se₁, In-Se₂) in Se octahedral sublattice and the other is van der Waals bonds (Se-Se) between the layers. Comparing the structures of phases I and II (Figs. 4(a) and 4(b)), we found that no obvious rotation or

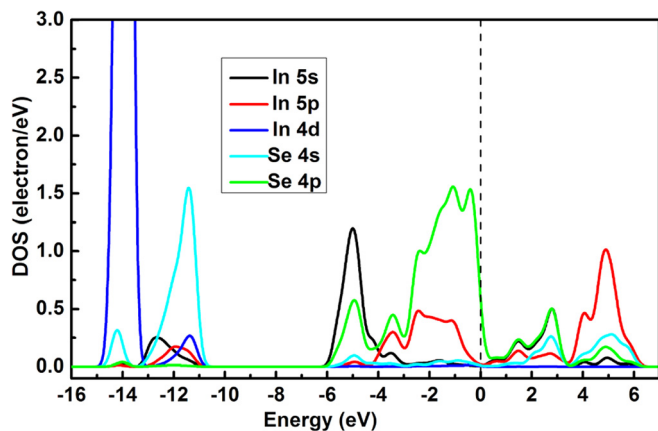


FIG. 3. Density of states (DOS) of In_2Se_3 at 0 GPa based on first-principle band structure calculation.

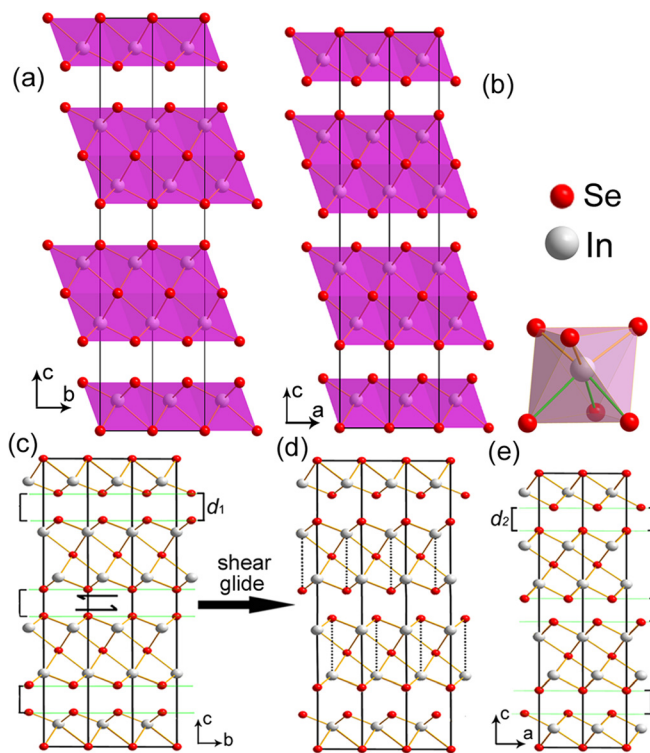


FIG. 4. (a) and (b) Polyhedral views of In_2Se_3 in phases I, II, and Se octahedral sublattice, respectively. The green and gold lines represent two types of covalent bonds In-Se₁ and In-Se₂. (c) Structure model of In_2Se_3 in phase I. (d) Interlayer shear gliding process of In_2Se_3 under pressure. (e) Structure model of In_2Se_3 in phase II.

distortion in Se octahedral sublattice. Therefore, the rotation or distortion of octahedral should not be the predominant reason for the large volume collapse in In_2Se_3 .

Fortunately, it can be seen from Figs. 4(c)–4(e) that if an interlayer shear glide takes place in In_2Se_3 under pressure, the structure of phase I transforms to a new structure that matches well with the structure of phase II. In In_2Se_3 , it is not difficult to drive this type of interlayer shear glide because the van der Waals bonds between adjacent layers are weak. Due to this interlayer shear glide, the outer Se atoms of one sheet site into the interstitial sites of outer Se atoms in neighboring sheet, which leads to a $\sim 10\%$ reduction in the interlayer distance. Within the experimental uncertainty, the reduction of interlayer distance shows better agreement with the phase transition-associated volume collapse. The large interlayer distance reduction is also consistent with the pronounced hardening of the A_{1g} Raman mode at 104 cm^{-1} in phase II, which represents the vibration of one layer against the others along c -axis. The interlayer shear glide induces amounts of structural defects, accounting for the observed peak broadening in the Raman spectra and XRD patterns of In_2Se_3 at phase II (Fig. 2(a)). As the sheets glide with respect to one another, the sites of Se atoms are replaced by the nearest In atoms, so that the symmetry of In_2Se_3 can be well protected. Therefore, we rationalize that the phase transition observed in In_2Se_3 at 0.8 GPa can be attributed to the pressure-induced interlayer shear glide.

When carefully examining the difference between phases I and II, we found that through the glide of sheet involves no symmetry change but affects the stacking sequence

substantially. As can be seen in Figs. 4(c) and 4(e), the initial regular stacking sequence Se(a)-In(b)-Se(c)-In(a)-Se(b)... Se(b)-In(c)-Se(a)-In(b)-Se(c)... Se(c)-In(a)-Se(b)-In(c)-Se(a)... Se(b)-In(c)-Se(a)-In(b)-Se(c). This stacking variation looks like the polytypic transitions happened, for instance, in SiC and TaS₂ where the stacking sequence changes in the phase transitions.²⁶⁻²⁸ But the remarkable difference is that the I-II isosymmetric transition in In₂Se₃ leaves crystal symmetry unaffected, whereas the polytypic transitions in SiC and TaS₂ result in the change of space group.

In summary, we observed an interlayer shear glide-induced isosymmetric phase transition along with a ~7% volume collapse in dense In₂Se₃. This shear glide changes the relative sites of the outer Se atoms from top of each other to the interstitial sites of three Se atoms in the neighboring sheet. So the stacking sequence of In₂Se₃ varies significantly. Interestingly, it does not break down the crystal symmetry. The structural evolution information gives an insight to the effects of stress environment on the structural and functional stability of In₂Se₃, which should be essential for exploring the practical application of In₂Se₃-based materials.

This work was supported by the National Basic Research Program of China (Grant No. 2011CB808204), National Natural Science Foundation of China (Grant Nos. 91014004, 11304114, and 11374121), China Postdoctoral Science Foundation (Grant No. 2013M540243), Program of Science and Technology Development Plan of Jilin Province (Grant No. 20140520105JH), and Fundamental Research Funds for Jilin University, China (Grant No. 450060491500).

¹A. G. Christy, *Acta Crystallogr., Sect. B: Struct. Sci.* **51**, 753 (1995).

²S. G. Louie and M. L. Cohen, *Phys. Rev. B* **10**, 3237 (1974).

³J.-F. Lin, G. Vanko, S. D. Jacobsen, V. Lota, V. V. Struzhkin, V. B. Prakapenka, A. Kuznetsov, and C.-S. Yoo, *Science* **317**, 1740 (2007).

⁴J. Haines, J. M. Leger, and O. Schulte, *Phys. Rev. B* **57**, 7551 (1998).

⁵F. Datchi, S. Ninet, M. Gauthier, A. M. Saitta, B. Canny, and F. Decremps, *Phys. Rev. B* **73**, 174111 (2006).

⁶J. M. Rondinelli and S. Coh, *Phys. Rev. Lett.* **106**, 235502 (2011).

⁷R. Aso, D. Kan, Y. Shimakawa, and H. Kurata, *Sci. Rep.* **3**, 2214 (2013).

⁸D. Bidjin, S. Popovic, and B. Celustka, *Phys. Status Solidi A* **6**, 295 (1971).

⁹H. L. Peng, C. Xie, D. T. Schoen, and Y. Cui, *Nano Lett.* **8**, 1511 (2008).

¹⁰S. Popovic, A. Tonejc, B. Grzeta-Plenkovic, B. Celustka, and R. Trojko, *J. Appl. Cryst.* **12**, 416 (1979).

¹¹J. Jasinski, W. Swider, J. Washburn, Z. Liliental-Weber, A. Chaiken, K. Nauka, G. A. Gibson, and C. C. Yang, *Appl. Phys. Lett.* **81**, 4356 (2002).

¹²Y. Li, J. Gao, Q. L. Li, M. F. Peng, X. H. Sun, Y. Y. Li, G. Yuan, W. Wen, and M. Meyyappan, *J. Mater. Chem.* **21**, 6944 (2011).

¹³X. Tao and Y. Gu, *Nano Lett.* **13**, 3501 (2013).

¹⁴B. Yu, S. Ju, X. H. Sun, G. Ng, T. D. Nguyen, M. Meyyappan, and D. B. Janes, *Appl. Phys. Lett.* **91**, 133119 (2007).

¹⁵Q. L. Li, Y. Li, J. Gao, S. D. Wang, and X. H. Sun, *Appl. Phys. Lett.* **99**, 243105 (2011).

¹⁶T. Y. Zhai, X. S. Fang, M. Y. Liao, X. J. Xu, L. Li, B. D. Liu, Y. Koide, Y. Ma, J. N. Yao, Y. Bando, and D. Golberg, *ACS Nano* **4**, 1596 (2010).

¹⁷K. Osamura, Y. Murakami, and Y. Tomiie, *J. Phys. Soc. Jpn.* **21**, 1848 (1966).

¹⁸J. Ye, S. Soeda, Y. Nakamura, and O. Niitono, *Jpn. J. Appl. Phys., Part 1* **37**, 4264 (1998).

¹⁹R. Lewandowska, R. Bacewicz, J. Filipowicz, and W. Paszkowicz, *Mater. Res. Bull.* **36**, 2577 (2001).

²⁰A. M. Rasmussen, S. T. Teklemichael, E. Mafi, Y. Gu, and M. D. McCluskey, *Appl. Phys. Lett.* **102**, 062105 (2013).

²¹H.-K. Mao, P. M. Bell, J. W. Shaner, and D. J. Steinberg, *J. Appl. Phys.* **49**, 3276 (1978).

²²M. D. Segall, P. J. D. Lindan, M. J. Probert, C. J. Pickard, P. J. Hasnip, S. J. Clark, and M. C. Payne, *J. Phys.: Condens. Matter* **14**, 2717 (2002).

²³J. P. Perdew, K. Burke, and M. Ernzerhof, *Phys. Rev. Lett.* **77**, 3865 (1996).

²⁴See supplementary material <http://dx.doi.org/10.1063/1.4879832> for the detailed structural information of In₂Se₃ in phases I and II obtained by the X-ray diffraction measurements and first-principle calculations.

²⁵R. Vilaplana, O. Gomis, F. J. Manjon, A. Segura, E. Perez-Gonzalez, P. Rodriguez-Hernandez, A. Munoz, J. Gonzalez, V. Marin-Borras, V. Munoz-Sanjose, C. Drasar, and V. Kucek, *Phys. Rev. B* **84**, 104112 (2011).

²⁶M. S. Miao and W. R. L. Lambrecht, *Phys. Rev. B* **68**, 092103 (2003).

²⁷C. W. Dunnill, I. Maclaren, and D. H. Gregory, *Nanoscale* **2**, 90 (2010).

²⁸J. V. Landuyt, G. V. Tendeloo, and S. Amelinckx, *Phys. Status Solidi A* **26**, 585 (1974).